PCCP

Physical Chemistry Chemical Physics

www.rsc.org/pccp

Volume 13 | Number 44 | 28 November 2011 | Pages 19643–20022

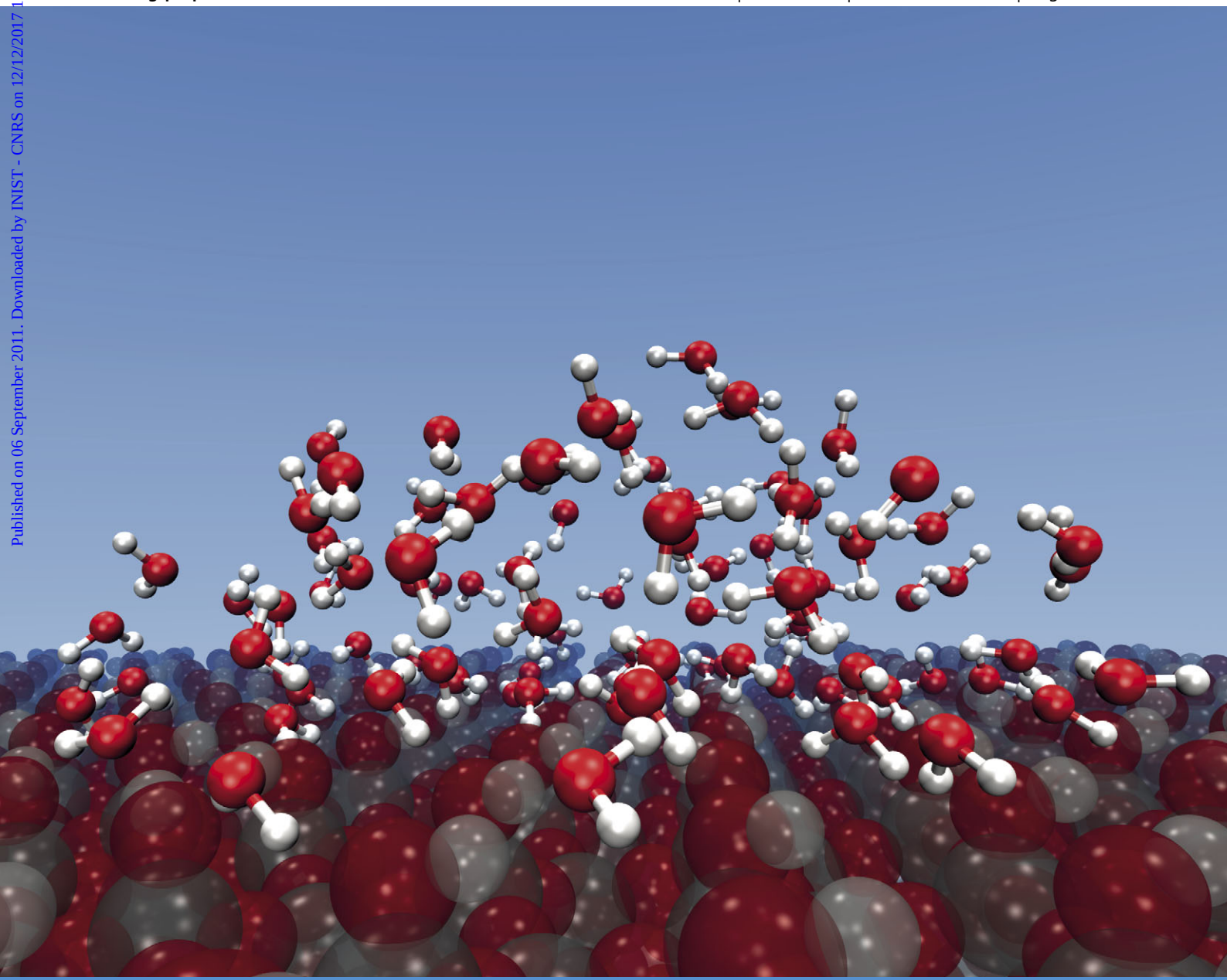

The physics and chemistry of ice and water

ISSN 1463-9076

COVER ARTICLE
Laage *et al.*
Non-monotonic dependence of water reorientation dynamics on surface hydrophilicity

PERSPECTIVE
Nezbeda and Jirsák
Water and aqueous solutions: simple non-speculative model approach

1463-9076(2011)13:44;1-Q

PCCP

Cite this: *Phys. Chem. Chem. Phys.*, 2011, **13**, 19911–19917

www.rsc.org/pccp

PAPER

Non-monotonic dependence of water reorientation dynamics on surface hydrophilicity: competing effects of the hydration structure and hydrogen-bond strength

Guillaume Stirnemann,*[a] Santiago Romero-Vargas Castrillón,[b] James T. Hynes,[ac] Peter J. Rossky,[d] Pablo G. Debenedetti*[b] and Damien Laage*[a]

Received 13th June 2011, Accepted 24th August 2011
DOI: 10.1039/c1cp21916b

The reorientation dynamics of interfacial water molecules was recently shown to change non-monotonically next to surfaces of increasing hydrophilicity, with slower dynamics next to strongly hydrophobic (apolar) and very hydrophilic surfaces, and faster dynamics next to surfaces of intermediate hydrophilicities. Through a combination of molecular dynamics simulations and analytic modeling, we provide a molecular interpretation of this behavior. We show that this non-monotonic dependence arises from two competing effects induced by the increasing surface hydrophilicity: first a change in the hydration structure with an enhanced population of water OH bonds pointing toward the surface and second a strengthening of the water–surface interaction energy. The extended jump model, including the effects due to transition-state excluded volume and transition-state hydrogen-bond strength, provides a quasi-quantitative description of the non-monotonic changes in the water reorientation dynamics with surface hydrophilicity.

1. Introduction

Understanding the influence of an interface on the dynamics of the vicinal water molecules is of great importance in many contexts, ranging from nanofluidics, where water flows within nanoscale channels,[1] to electrochemistry at metallic interfaces and electrodes,[2] to biochemistry, including lipid bilayer,[3] reverse micelle[4] and protein interfaces,[5,6] where hydration dynamics plays a critical role in the biochemical and biophysical properties. The impact of a surface on water dynamics can be described by two essential properties: its topology, *e.g.* flat *vs.* rough, and its interaction energy with water, *e.g.* hydrophobic *vs.* hydrophilic character, determined by the chemical nature of the surface exposed groups.[7,8] While a series of studies have greatly improved the understanding of the structural and thermodynamic properties of water at interfaces, both experimentally[9,10] and through numerical simulations,[11–15] the dynamical aspects have remained comparatively more elusive.[16–19]

A recent computational study of the impact of surface polarity on the interfacial water dynamics has led to surprising results.[18] When an initially hydrophobic surface was progressively turned into a more hydrophilic surface, the interfacial water dynamics was shown to first accelerate before slowing down for very hydrophilic surfaces.

Here, we employ molecular dynamics simulations and analytic models to provide a molecular interpretation of this non-monotonic behavior. Our analysis relies on the extended molecular jump model[20] to predict the impact of different surfaces on the vicinal water reorientation dynamics, and extends to the hydrophilic surface case a previous detailed study of water reorientation and hydrogen-bond (HB) dynamics next to a hydrophobic interface.[21]

The remainder of this paper is organized as follows. Section 2 describes the system made of water confined between two plates of varying hydrophilicity, and the details of the molecular dynamics simulations. The hydration structure and its dependence on the surface hydrophilicity are analyzed in Section 3. The dynamics of interfacial water molecules is presented in Section 4, which describes both the direct calculation of the reorientation times and their analysis through the extended jump model. Section 5 then explains the origin of the observed non-monotonic dependence of water dynamics on surface hydrophilicity. We end with some concluding remarks.

2. System and methodology

2.1 System and simulations

Our present analysis relies on the same simulations as in prior work, where an extensive description of the simulations has been provided.[11,12,18] We summarize the key points here.

[a] *Chemistry Department, Ecole Normale Supérieure, UMR ENS-CNRS-UPMC 8640, 24 rue Lhomond, Paris, France. E-mail: guillaume.stirnemann@ens.fr, damien.laage@ens.fr; Tel: + 33 1 44 32 24 18*
[b] *Dept. of Chemical and Biological Engineering, Princeton University, Princeton, NJ, USA. E-mail: pdebene@princeton.edu*
[c] *Dept. of Chemistry and Biochemistry, University of Colorado, Boulder, CO, USA*
[d] *Dept. of Chemistry and Biochemistry, University of Texas, Austin, TX, USA*

The system consists in a slab of water taken from a simulation of bulk water at a 1 g.cm^{-3} density, confined between two β-cristobalite plates. The rigid, non-polarizable SPC/E model is used for water molecules.[22] While other water potentials, including *e.g.* the TIP4P/2005 model,[23] provide a better description of the full phase diagram, we have used the SPC/E potential for consistency with prior work[18] and because it was shown to yield water reorientation and HB dynamics in quantitative agreement with experiments[24] under the ambient conditions where our study is performed. Each plate contains four layers of silica SiO_2, reproducing the (1.1.1) octahedral face of β-cristobalite.[11] Hydrophilic plates are then generated by totally hydroxylating the surfaces. All tetrahedra are idealized as perfect, with O–O and Si–O distances equal to 0.247 and 0.151 nm, respectively, and a O–Si–O angle of 129°28′. As with hydrogen atoms in the SPC/E model, hydrogen atoms on the surface do not interact *via* Lennard-Jones potentials. On the surface, the O–H distance is fixed at 0.1 nm as in the SPC/E model, and the Si–O–H angle is equal to 129°28′. Thus, the H atom plane is located at a 0.033 nm distance from the O atom plane of the surface. Whereas Si and O atoms are not allowed to move, H atoms can reorient while maintaining the O–H distance and the Si–O–H valence angle constant. Lennard-Jones parameters for the surface atoms can be found elsewhere.[11,18]

The series of plates with different hydrophilicities are generated from the fully hydroxylated plates. Following an approach already successfully used by some of us,[11,18] the surface polarity and thus its hydrophilic/hydrophobic character are modulated by rescaling the charges of all atoms (Si, O and H) within the wall interfacial layer by a factor k so that $q_i = k \times q_{0,i}$, where $q_{0,i}$ denotes the charge of atom i in the fully hydroxylated case. Thus, plates with $k = 0$ are hydrophobic (wall atoms interact with water molecules exclusively through Lennard-Jones potentials), hydrophilic plates correspond to $k = 1$ and intermediate cases to $0 < k < 1$. For convenience, the hydrophobic plate is modeled using the fully hydroxylated plate with $k = 0$ instead of a non-hydroxylated plate.

We use square plates of length 6.93 nm in the x and y directions, which corresponds to the box size, so that the plates are infinite in these directions because of periodic boundary conditions. The plate separation along the z direction, taken between the H atom planes, is fixed at 1.6 nm. Previous studies have shown that this separation is sufficient to observe the transition from wall-dominated water dynamics next to the interface to bulk-like rotational dynamics away from the surfaces.[18] In our analysis, the distance to the surface is defined as the distance to the H atom plane.

Molecular dynamics simulations are performed in the canonical NVT ensemble, with the temperature fixed at 300 K by a Berendsen thermostat with a 1 ps coupling time. The interval between each saved configuration is 1 ps, while the propagation time step is 1 fs. Trajectories are typically run for 1 ns.

2.2 Calculation of hydrogen-bond jump exchange times

The HB jump exchange time is defined as the average time for a water OH to go from a stable initial HB acceptor to a new stable HB acceptor.[25,26] This HB acceptor exchange process can be fruitfully viewed as a chemical reaction, whose forward rate constant is the inverse jump time. As detailed in Section 4, the reorientation time is related to the jump time. Following previous work,[26] stable HB configurations are used for the initial and final states and are defined by tight geometric HB conditions ($R_{OO} < 3.0$ Å, $R_{OH} < 2.0$ Å, $\theta_{HOO} < 20°$, where H and O can refer to either a surface silanol or a water molecule OH.). The jump time τ_{jump} is calculated through the cross time-correlation function between the initial (I) and final (F) states as $\langle p_I(0)\, p_F(t)\rangle = 1-\exp(-t/\tau_{jump})$, where $p_I(t)$ is 1 if the system is in state I at time t and 0 otherwise, and correspondingly for $p_F(t)$. States I and F are defined within the Stable States Picture[27] to remove the contributions from fast barrier recrossing[25,26] and absorbing boundary conditions in the product state ensure that the forward rate constant is calculated. Several key geometric features of these jumps, including *e.g.* their amplitude, can then be determined from the simulations.[26]

3. Structure of the water interface

The reorientation dynamics of an interfacial water molecule was recently shown to sensitively depend both on its orientation relative to the interface and on the nature of its HB partners.[21,25,28–30] We therefore first characterize the structure of the water HB network next to the interface.

A detailed study of the changes in the water structure induced by an increasingly hydrophilic interface has already been presented by some of us for the same set of surfaces.[11,18] We now summarize these prior results and complement them to determine the key structural features necessary to understand the reorientation dynamics.

The thickness of the interfacial water layer is determined from the first minimum in the water oxygen density profile along the surface normal. As already recognized,[11,18] this thickness decreases with increasing surface hydrophilicity due to the greater water molecule localization with increasing water–surface attraction (Fig 1a).

Within the interfacial layer, the water OH bonds have different preferred orientations, which significantly change with the surface hydrophilicity. This clearly appears in the probability distributions of water OH bond orientations as a function of the distance to the interface, plotted for each surface in Fig. 1b.

Next to the most hydrophobic surface ($k = 0$), the first hydration layer is broad (2.7 Å thick[31]) and OH bonds exhibit three preferred orientations (Fig 1c): (a) water OHs pointing toward the surface and lying very close to it, usually referred to as dangling OHs; (b) OHs lying tangent to the interface, which represent the major fraction of the first hydration layer, and which donate a HB to other water molecules within the interfacial hydration layer; (c) OHs donating a HB to water molecules lying within the second layer and pointing away from the interface. These three distinct peaks are a signature of a spatial alternation of anti-clathrate and clathrate like arrangements in the first hydration layer.[14,21] A detailed description of HB exchange dynamics between these populations next to such an extended hydrophobic surface has already been presented.[21]

We now contrast these results with the other extreme, the most hydrophilic surface ($k = 1$). The first hydration layer is closer to the surface and more compact (2.0 Å thick) than in

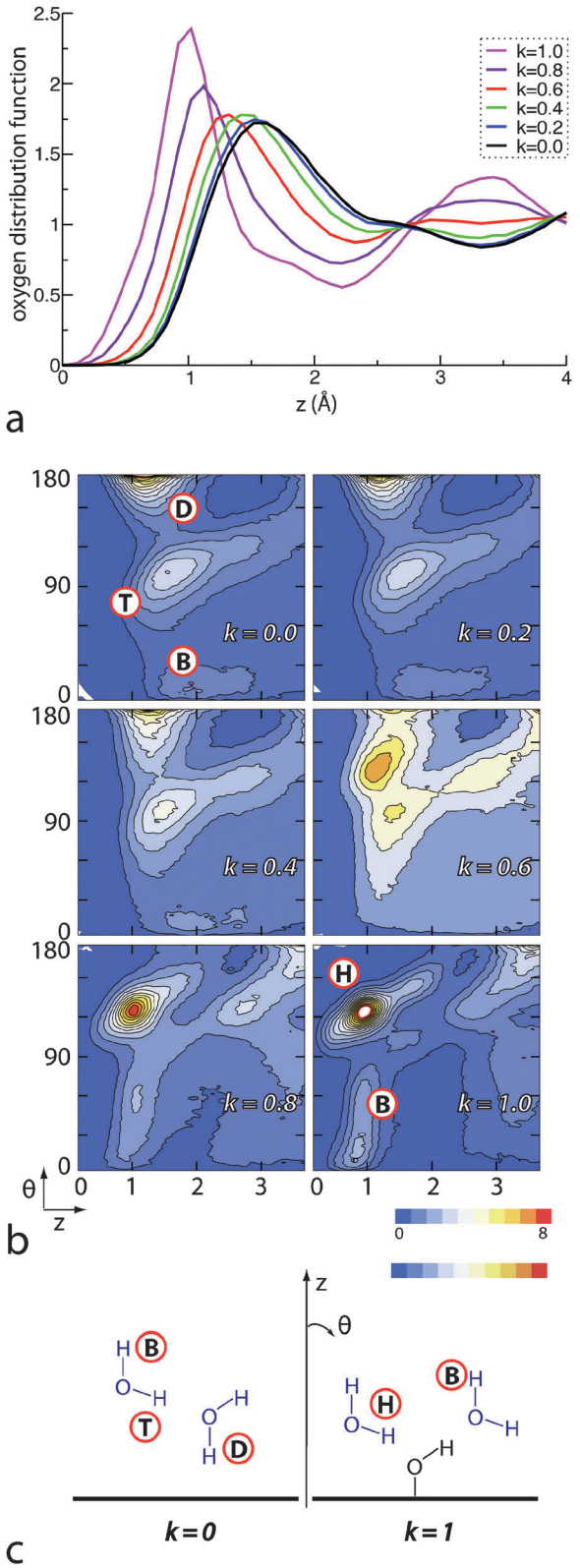

Fig. 1 (a) Water oxygen distribution function along the axis normal to the interfacial plane for different surface hydrophilicities. (b) Normalized probability distribution for the angle between a water OH and the surface normal vector along the distance to the surface plane. (c) Schematic description of the different preferred OH orientations indicated in panel (b): dangling (D), tangent to the interface (T), and donating a HB, respectively, to a surface hydroxyl (H) and a bulk water molecule (B).

the hydrophobic case. Three preferred OH orientations are now distinguishable: (a) OHs donating a HB to the surface hydroxyl oxygens and pointing toward the surface at a 120° angle because of the tetrahedral environment imposed by the surface hydroxyls; (b) OHs pointing away from the surface and whose orientation is broadly spread; (c) a very small fraction of OHs lying tangent to the interface. We note that the peak associated with dangling OHs facing the surface has totally disappeared. These changes in the hydration layer structure mainly reflect the formation of HBs donated by water OHs to the surface, as shown in Fig. 2. The additional HBs donated by the surface hydroxyls to the interfacial water molecules[16,18,32] do not lead to a strong orientational preference of the water OH, as manifested by the broad B peak in Fig. 1b.

For intermediate hydrophilicity values, the two-dimensional probability distributions in Fig. 1bshow that the hydration structure continuously evolves between the two extreme cases detailed above. With increasing k, the intensity of the dangling peak decreases and eventually disappears for $k > 0.4$. In addition, the formation of HBs with the surface oxygen atoms (Fig. 2) gives rise to the peaks characterizing the hydrophilic hydration structure, for $k > 0.6$. As previously evidenced,[11,18] the turnover between pronounced hydrophobic and hydrophilic behaviors occurs between $k = 0.4$ and $k = 0.6$.

4. Dynamics of interfacial water molecules

4.1 Reorientation dynamics

Now that the effect of different surface hydrophilicities on the hydration structure has been established, we turn to the impact of hydrophilicity on the reorientation dynamics of water OHs lying within the interfacial layer.

Water reorientation can be followed using the second-order Legendre polynomial time-correlation function

$$C(t) = \langle P_2 [\mathbf{u}(0)\cdot\mathbf{u}(t)] \rangle, \quad (1)$$

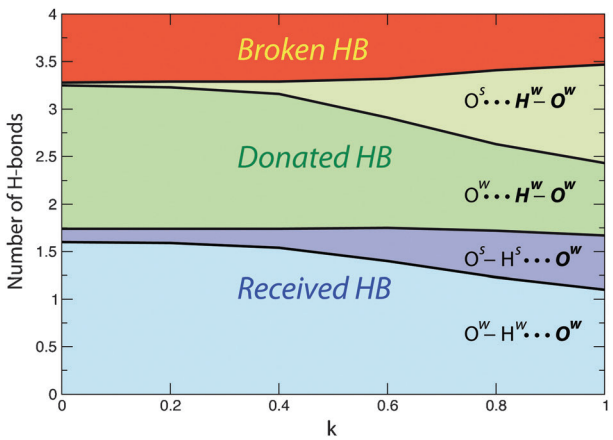

Fig. 2 Total number of received, donated and broken hydrogen-bonds per interfacial water molecule for increasing surface hydrophilicity. For each received and donated bond, the type of hydrogen-bond partner, either belonging to the surface (S) or to another water (W), is specified. Here, standard geometric criteria are employed to define a hydrogen-bond ($R_{OO} < 3.5$ Å, $R_{OH} < 2.45$ Å, $\theta_{HOO} < 30°$).

where $\mathbf{u}(t)$ designates the orientation of the water OH bond at time t. This function is of particular interest since it can be related to experimental observables in NMR[33] and ultrafast infrared spectroscopy.[34,35]

In bulk water and at ambient temperature, $C(t)$ exhibits a fast initial drop (<200 fs) due to librations[36] and subsequently decreases exponentially with a 2.5 ps time constant. The reorientation time determined from simulations with the SPC/E model[26] is in excellent agreement with the experimental values, both from NMR[33] and ultrafast IR spectroscopies.[34,35]

For water OHs initially within the interfacial layer, the average orientational time-correlation function decays more slowly than in the bulk at all values of the hydrophilicity k parameter (Fig. 3). The inset in Fig. 3 shows the dependence of the effective reorientation time, determined from an exponential fit of $C(t)$ on the 2–10 ps interval, on the hydrophilicity k parameter. As already pointed out in earlier studies of the water dipole relaxation time next to the same surfaces,[18] the reorientation time does not evolve monotonically with k. Next to a purely hydrophobic interface ($k = 0$), the water reorientation dynamics is almost twice as slow as in the bulk, consistently with previous work.[21,28] With increasing surface hydrophilicity, the retardation factor compared to the bulk value first decreases to reach a 1.2 minimum for $k = 0.6$, before increasing to 2.75 for $k = 1$ (full surface charges). We stress that this range of retardation factors is fully consistent with the 1.5–2.5 range of values which have been measured by NMR for the water reorientation dynamics next to small hydrophobic peptides[37] and next to larger proteins including *e.g.* BPTI and ubiquitin,[38] whose solvent-exposed surfaces include hydrophobic patches and hydrophilic sites.

As shown in Fig. 3, these reorientational decays exhibit a non-exponential character, which suggests that the average over the interfacial layer includes different types of OHs with distinct reorientation times. In order to connect these different dynamics to the distinct populations and structural arrangements described in Section 3, we will employ the recently suggested molecular jump picture, whose description of the reorientation mechanism as a chemical reaction provides a framework to predict the impact of the local environment on the reorientation kinetics.[20]

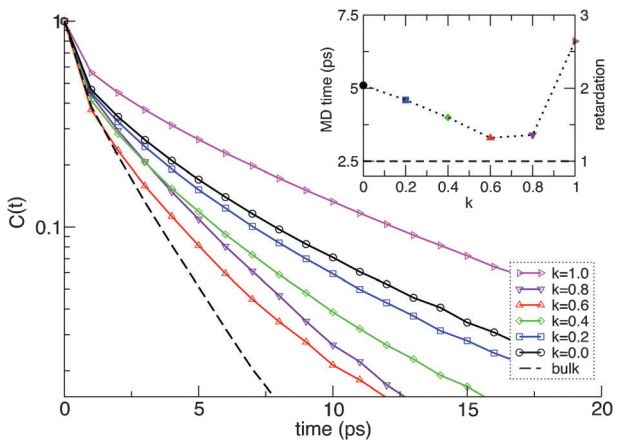

Fig. 3 Orientational time-correlation functions eqn (1) for a water OH bond initially within the interfacial layer, plotted for different surface hydrophilicities. The inset shows the values of the characteristic decay time determined from an exponential fit on the 2–10 ps interval, and its ratio with the bulk reference value which is the surface-induced retardation factor.

4.2 Extended jump model

In contrast to the traditional rotational diffusion picture, it was recently shown that beyond the initial fast librational decay, water reorientation mainly occurs through large amplitude jumps due to the exchange of HB acceptors.[20,25,26] It is only once the environment has reorganized to offer a new stable HB acceptor that the water OH bond quickly executes a large-amplitude angular jump from its former HB partner to this new acceptor. This HB acceptor exchange can be fruitfully seen as a chemical reaction. The characteristic time of the resulting orientational relaxation for the correlation function in eqn (1) was shown to be well described by an analytic extended jump model,[25,26] which combines the jump reorientation together with the slower diffusive tumbling time τ_{frame} of the coordinate frame for a water OH engaged in an intact HB between jump events,

$$\frac{1}{\tau_{\text{reor}}} = \frac{1}{\tau_{\text{jump}}}\left[1 - \frac{1}{5}\frac{\sin(5\Delta\theta/2)}{\sin(\Delta\theta/2)}\right] + \frac{1}{\tau_{\text{frame}}}. \qquad (2)$$

The two key ingredients entering into the dominant jump contribution are the jump time τ_{jump}, *i.e.* the inverse jump HB exchange rate constant, and the average jump amplitude $\Delta\theta$.

Studies of water reorientation next to a wide range of solutes and interfaces have shown that the changes in the water reorientation dynamics mainly result from a change in the jump time.[21,25,39,28–30] For a water molecule lying at the interface between a solute and the bulk, it has been shown that the jump time depends on two factors, the local topology and the strength of the HB to be broken.[20] We now describe these two factors, which will be used to understand the changes in the jump times with the surface hydrophilicity.

4.3 Transition-state excluded volume (TSEV)

The first effect is topological and is induced by any type of solute and interface. It results from the partial hindrance of a new water HB partner's approach. Compared to the bulk situation, the volume occupied by the solute reduces the number of accessible transition state (TS) configurations for the jump exchange and leads to a slowdown in the jump rate.[21,28] The resulting transition-state excluded volume (TSEV) slowdown factor ρ_{V} is quantitatively determined by the fraction f of the transition-state locations forbidden by the solute/surface excluded volume,[21,28]

$$\rho_{\text{V}} = \frac{\tau_{\text{jump}}^{\text{interface}}}{\tau_{\text{jump}}^{\text{bulk}}} = \frac{1}{1-f}, \qquad (3)$$

in which $\tau_{\text{jump}}^{\text{interface}}$ designates the jump time to a new HB partner in the presence of the solute/surface, while $\tau_{\text{jump}}^{\text{bulk}}$ is the reference jump time in the bulk.

Typical TSEV slowdown factors determined in prior studies range from approximately 1.4 next to convex surfaces[28] (*e.g.* around small isolated solutes), where less than half of

the space is forbidden in the TS, to 1.8 next to a flat extended hydrophobic surface.[21]

4.4 Transition-state hydrogen-bond strength (TSHB)

The second main factor which affects the jump time is the strength of the initial HB which must be elongated to reach the jump TS configuration. This factor differs from 1 only when the initial HB acceptor is not a water oxygen. Compared to the bulk situation, this transition-state hydrogen-bond (TSHB) strength factor ρ_{HB} can either accelerate the jump rate if the initial bond is weaker than a water–water HB, or slow it down if the initial bond to the surface is stronger. This ρ_{HB} factor is quantitatively given by[29]

$$\rho_{HB} = \exp\left[(\Delta G^{\ddagger}_{S} - \Delta G^{\ddagger}_{water})/RT\right], \quad (4)$$

where $\Delta G^{\ddagger}$ is the free energy cost to stretch the initial HB with a surface (or with a water) HB acceptor to its TS length.

Typical TSHB factors determined in prior studies on a wide range of HB acceptor sites range from 0.5 (*i.e.* a two-fold acceleration) up to a 4-fold slowdown.[29]

Returning to the general case of a water molecule at the interface between a solute and the bulk, the jump time results from the combination of the TSEV and TSHB factors,

$$\tau_{jump} = \rho_{V}\, \rho_{HB}\, \tau^{bulk}_{jump}. \quad (5)$$

We now apply this model to understand the non-monotonic dependence of the water reorientation time on the surface hydrophilicity.

5. Explanation of non-monotonic hydrophilicity dependence

5.1 Kinetic model

The different preferred OH orientations within the interfacial layer identified in Section 3 reveal distinct states with different local environments and thus different reorientation times. For simplicity, we use here a simplified version of a previous study by some of us of water dynamics next to a purely hydrophobic surface.[21] We classify the interfacial water OHs into two categories, according to whether they donate a HB to another water (state **W**) or point to a surface oxygen (state **S**). State **W** thus includes the bulk (B) and tangent (T) orientations identified in Fig. 1, while state **S** includes the dangling (D) configuration in the hydrophobic case and the hydroxyl-bonded systems (H) in the hydrophilic situation. HB exchanges both between these states and within these states lead to reorientation of the water OH bond.

5.2 Change in the hydration structure

The main structural consequence of an increase in the surface hydrophilicity is an increase in the relative population of interfacial water OHs within the **S** state, pointing to the surface which is an increasingly good HB acceptor. As shown in Fig. 4a, the population in the **S** state increases from less than 3% in the purely hydrophobic case to 60% in the most hydrophilic situation.

5.3 Change in HB strength

We now turn to the impact of the increasing surface hydrophilicity on the reorientation time of a water OH initially in the **S** or **W** state. As explained in Section 4, the reorientation dynamics is dominated by the jump reorientation component, which is governed by the jump exchange time between HB acceptors.

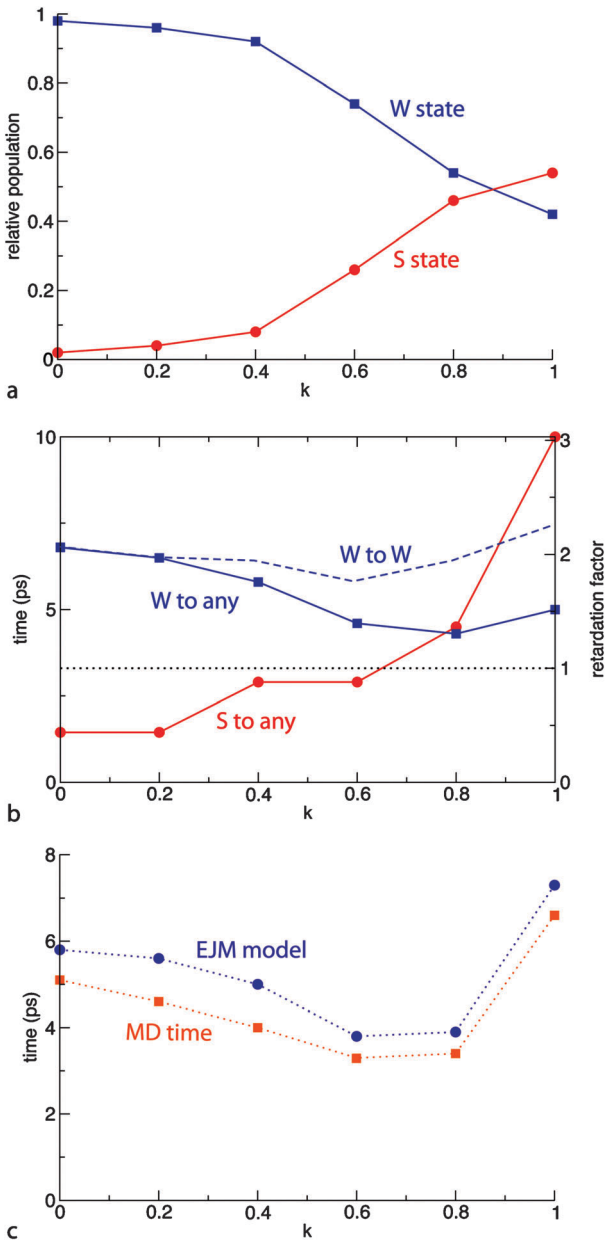

Fig. 4 (a) Relative fractions of interfacial water OH bonds which, respectively, donate a HB to a water oxygen (state **W**) or point to a surface site (state **S**), *versus* the surface hydrophilicity. (b) HB jump exchange time for a water OH initially in state **W** or **S**. (c) Average reorientation times for an interfacial water OH, either computed directly (MD time, see inset in Fig. 3) or calculated through the extended jump model (EJM) with the **S**/**W** two-state picture, using the jump times shown in panel (b), the populations in panel (a), the 68° bulk jump amplitude and the tumbling times of intact HB axes computed directly.

For a water OH initially in state **W**, Fig. 4b shows that the jump time is weakly sensitive to the surface polarity. This can be explained by the following considerations. In state **W**, the HB acceptor is a water oxygen; there is therefore no contribution from the TSHB factor and the changes in the jump time exclusively originate from the TSEV slowdown. For a jump from a water acceptor to another water acceptor, the TSEV slowdown factor changes very little with the surface hydrophilicity, since most of the **W** population is approximately tangent to the interface that excludes close to half the local space. This leads to an average TSEV slowdown factor close to 2 for any surface hydrophilicity, in agreement with the **W** → **W** time reported in Fig. 4b. However, for increasing hydrophilicities, the surface sites become possible HB acceptors and jumps can occur from the **W** to the **S** state, which accelerates slightly the overall jump time for **W**, as shown in Fig. 4b.

In contrast, within state **S**, the jump time exhibits a dramatic slowdown with increasing surface hydrophilicity, due to large changes in the TSHB factor. In the hydrophobic situation ($k = 0$), the nonexistent initial HB implies that there is no free-energy cost to stretch the initial bond to reach the TS configuration, which leads to a two-fold acceleration compared to the bulk case. With increasing surface hydrophilicity, the jump time slows down but remains faster than in the bulk until $k > 0.6$. For greater hydrophilicities, stretching the initial HB leads to a free energy cost greater than that of elongating a water–water bond, and the jump time then becomes slower than the bulk time, culminating at a three-fold slowdown for $k = 1$. The jump time starting from the **S** state also includes a contribution from the TSEV factor, but the latter is nearly independent of the surface hydrophilicity, as for the **W** case, and remains close to $\rho_V = 1.3$. We note that the formation of strong HB with hydrophilic surfaces and their impact on water reorientation dynamics has also been evidenced for other systems, including *e.g.* inorganic oxides simulated with *ab initio* molecular dynamics,[40] clays[41] or other silica surfaces.[16,17]

5.4 Non-monotonic behavior

The origin of the non-monotonic dependence of the interfacial water dynamics on the surface hydrophilicity can now be assigned to the combined but competing effects of the hydrophilicity on the hydration structure, *i.e.* on the relative populations within the **S** and **W** states, and on the reorientation time for a OH within the **S** state. Starting from a purely hydrophobic surface, increasing the hydrophilicity leads to an acceleration of the water dynamics due to a greater fraction of the interfacial water OHs pointing toward the surface (state **S**) where they reorient quickly because the interaction with the surface is weak (Fig. 4b). The subsequent slowdown for greater surface hydrophilicities originates from the increasing HB strength in this state, which leads to a reorientation slower than in the bulk; this effect is amplified by the continuing growth of the interfacial water OH population forming HBs with the surface (Fig. 4a). Fig. 4c shows the average reorientation time within the interfacial layer determined from the **S** and **W** populations determined in Fig. 4a together with the **S** and **W** reorientation times calculated through the extended jump model with the jump times shown in Fig. 4b. These results evidence that this simplified two-state model provides a nearly quantitative description of the interfacial water reorientation time and of its non-monotonic dependence on the surface hydrophilicity.

We now contrast this non-monotonic behavior with a different situation where the *average* surface hydrophilicity is changed by adding surface groups with a fixed hydrophilicity. This has, for example, been done by increasing the fraction of hydroxylated surface oxygens.[16] In this case, the interfacial water dynamics was observed to vary monotonically with the surface density of these hydrophilic groups. This can be explained by our same picture, noticing that here the water–surface interaction strength remains constant, and that only the populations in the **S** and **W** states change with the average surface hydrophilicity, leading to a monotonic change. While in ref. 16 the water dynamics was observed to slow down when the fraction of hydroxylated oxygens increases, our picture suggests that using weak HB acceptor groups could lead to a monotonic acceleration of the interfacial water dynamics.

Conclusions

Based on molecular dynamics simulations and analytic modeling, we have determined why the water reorientation dynamics within the interfacial layer does not vary monotonically with the surface hydrophilicity. We have shown that two types of water OH bonds should be distinguished, with different reorientation times due to their different local environments: first the OHs pointing toward the surface and then the OHs donating a HB to another water. We have shown that two competing effects come into play: first a structural rearrangement of the hydration layer, where an increasing fraction of the water OHs point toward the surface when its hydrophilicity increases, and secondly a dynamic effect, where the reorientation time of this latter population becomes slower when the surface hydrophilicity increases, due to the greater interaction energy. The extended jump model together with the transition-state excluded volume and transition-state hydrogen-bond effects were shown to provide a quite accurate quantitative description of the changes in the reorientation times with the surface hydrophilicity. Our present conclusions should be of importance for the understanding of water dynamics next to metallic interfaces, electrodes, and biomolecular surfaces, including, *e.g.*, proteins and lipid bilayers, and can provide intuitive insights into the reorientation of water at water–liquid surfaces.[42]

Acknowledgements

We thank Nicolás Giovambattista for providing the code used in generating the MD trajectories. This work was supported in part by NSF grant CHE-0750477 (JTH). P.G.D. and P.J.R. gratefully acknowledge the support of the National Science Foundation (Collaborative Research Grants CHE-0908265 and CHE-0910615). Additional support from the R. A. Welch Foundation (F-0019) to P.J.R. is also gratefully acknowledged.

Notes and references

1 H. A. Stone, A. D. Stroock and A. Ajdari, *Annu. Rev. Fluid Mech.*, 2004, **36**, 381–411.
2 A. P. Willard, S. K. Reed, P. A. Madden and D. Chandler, *Faraday Discuss.*, 2009, **141**, 423–441.
3 S. Y. Bhide and M. L. Berkowitz, *J. Chem. Phys.*, 2006, **125**, 094713.
4 E. E. Fenn, D. B. Wong and M. D. Fayer, *Proc. Natl. Acad. Sci. U. S. A.*, 2009, **106**, 15243–15248.
5 P. Ball, *Chem. Rev.*, 2008, **108**, 74–108.
6 Y. Levy and J. N. Onuchic, *Annu. Rev. Biophys. Biomol. Struct.*, 2006, **35**, 389–415.
7 F. Pizzitutti, M. Marchi, F. Sterpone and P. J. Rossky, *J. Phys. Chem. B*, 2007, **111**, 7584–7590.
8 Y. K. Cheng and P. J. Rossky, *Nature*, 1998, **392**, 696–699.
9 Y. R. Shen and V. Ostroverkhov, *Chem. Rev.*, 2006, **106**, 1140–1154.
10 L. J. Michot, F. Villieras, M. Francois, I. Bihannic, M. Pelletier and J. M. Cases, *C. R. Geosci.*, 2002, **334**, 611–631.
11 N. Giovambattista, P. G. Debenedetti and P. J. Rossky, *J. Phys. Chem. B*, 2007, **111**, 9581–9587.
12 N. Giovambattista, P. G. Debenedetti and P. J. Rossky, *J. Phys. Chem. C*, 2007, **111**, 1323–1332.
13 M. Maccarini, *Biointerphases*, 2007, **2**, MR1–MR15.
14 C. Y. Lee, J. A. McCammon and P. J. Rossky, *J. Chem. Phys.*, 1984, **80**, 4448–4455.
15 J. Mittal and G. Hummer, *Faraday Discuss.*, 2010, **146**, 341–352.
16 D. Argyris, D. R. Cole and A. Striolo, *J. Phys. Chem. C*, 2009, **113**, 19591–19600.
17 D. Argyris, T. A. Ho, D. R. Cole and A. Striolo, *J. Phys. Chem. C*, 2011, **115**, 2038–2046.
18 S. R. V. Castrillon, N. Giovambattista, I. A. Aksay and P. G. Debenedetti, *J. Phys. Chem. B*, 2009, **113**, 1438–1446.
19 E. Mamontov, *J. Chem. Phys.*, 2004, **121**, 9087–9097.
20 D. Laage, G. Stirnemann, F. Sterpone, R. Rey and J. T. Hynes, *Annu. Rev. Phys. Chem.*, 2011, **62**, 395–416.
21 G. Stirnemann, P. J. Rossky, J. T. Hynes and D. Laage, *Faraday Discuss.*, 2010, **146**, 263–281.
22 H. J. C. Berendsen, J. R. Grigera and T. P. Straatsma, *J. Phys. Chem.*, 1987, **91**, 6269–6271.
23 C. Vega, E. Sanz, J. L. F. Abascal and E. G. Noya, *J. Phys.: Condens. Matter*, 2008, **20**, 153101.
24 J. R. Schmidt, S. T. Roberts, J. J. Loparo, A. Tokmakoff, M. D. Fayer and J. L. Skinner, *Chem. Phys.*, 2007, **341**, 143–157.
25 D. Laage and J. T. Hynes, *Science*, 2006, **311**, 832–835.
26 D. Laage and J. T. Hynes, *J. Phys. Chem. B*, 2008, **112**, 14230–14242.
27 S. H. Northrup and J. T. Hynes, *J. Chem. Phys.*, 1980, **73**, 2700–2714.
28 D. Laage, G. Stirnemann and J. T. Hynes, *J. Phys. Chem. B*, 2009, **113**, 2428–2435.
29 F. Sterpone, G. Stirnemann, J. T. Hynes and D. Laage, *J. Phys. Chem. B*, 2010, **114**, 2083–2089.
30 G. Stirnemann, J. T. Hynes and D. Laage, *J. Phys. Chem. B*, 2010, **114**, 3052–3059.
31 Because the one-dimensional profile in Fig. 1a exhibits a shoulder instead of a clear minimum for $k = 0$, the layer thickness is in this case best determined from the two-dimensional surface in Fig. 1b.
32 J. W. Wang, A. G. Kalinichev and R. J. Kirkpatrick, *J. Phys. Chem. C*, 2009, **113**, 11077–11085.
33 R. Ludwig, F. Weinhold and T. C. Farrar, *J. Chem. Phys.*, 1995, **103**, 6941–6950.
34 S. Park, D. E. Moilanen and M. D. Fayer, *J. Phys. Chem. B*, 2008, **112**, 5279–5290.
35 Y. L. A. Rezus and H. J. Bakker, *J. Chem. Phys.*, 2005, **123**, 114502.
36 D. Laage and J. T. Hynes, *Chem. Phys. Lett.*, 2006, **433**, 80–85.
37 J. Qvist and B. Halle, *J. Am. Chem. Soc.*, 2008, **130**, 10345–10353.
38 C. Mattea, J. Qvist and B. Halle, *Biophys. J.*, 2008, **95**, 2951–2963.
39 D. Laage and J. T. Hynes, *Proc. Natl. Acad. Sci. U. S. A.*, 2007, **104**, 11167–11172.
40 N. Kumar, S. Neogi, P. R. C. Kent, A. V. Bandura, J. D. Kubicki, D. J. Wesolowski, D. Cole and J. O. Sofo, *J. Phys. Chem. C*, 2009, **113**, 13732–13740.
41 V. Marry, B. Rotenberg and P. Turq, *Phys. Chem. Chem. Phys.*, 2008, **10**, 4802–4813.
42 G. L. Richmond and F. G. Moore, *Acc. Chem. Res.*, 2008, **41**, 739–748.